The Size-Dependent Accuracy of Nanoscale Thermometers.

ARTICLE *in* THE JOURNAL OF PHYSICAL CHEMISTRY B · SEPTEMBER 2014

Impact Factor: 3.3 · DOI: 10.1021/jp508047q · Source: PubMed

2 AUTHORS, INCLUDING:

David M Leitner
University of Nevada, Reno
112 PUBLICATIONS **2,934** CITATIONS

THE JOURNAL OF PHYSICAL CHEMISTRY B

Article

pubs.acs.org/JPCB

Size-Dependent Accuracy of Nanoscale Thermometers

Robert Alicki*[,†,‡] and David M. Leitner*[,‡,§]

[†]Institute of Theoretical Physics and Astrophysics, University of Gdansk, Gdansk, Poland

[§]Department of Chemistry and Chemical Physics Program, University of Nevada, Reno, Nevada 89557, United States

[‡]Freiburg Institute for Advanced Studies (FRIAS), University of Freiburg, Freiburg, Germany

ABSTRACT: The accuracy of two classes of nanoscale thermometers is estimated in terms of size and system-dependent properties using the spin-boson model. We consider solid state thermometers, where the energy splitting is tuned by thermal properties of the material, and fluorescent organic thermometers, in which the fluorescence intensity depends on the thermal population of conformational states of the thermometer. The results of the theoretical model compare well with the accuracy reported for several nanothermometers that have been used to measure local temperature inside living cells.

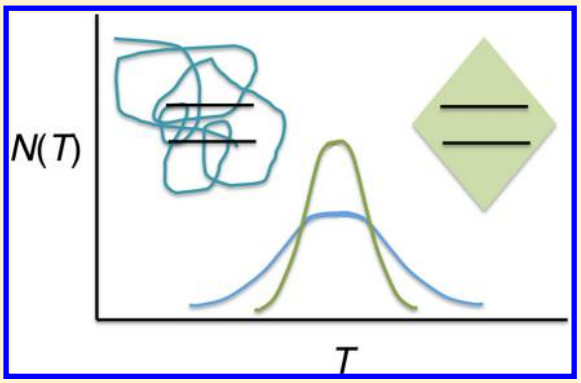

1. INTRODUCTION

Recent efforts to measure the temperature inside cells and other materials have led to development of a variety of nanoscale thermometers.[1−4] Thermometers designed and applied to measure local temperature within a living cell include fluorescent polymers[5,6] and proteins,[7] ratiometric fluorescent thermometers,[8] polymer dots,[9] fluorescent nanoparticles,[10,11] quantum dots,[12−14] and nanoscale diamonds.[15] The accuracy of each thermometer varies significantly. For example, a nanoscale diamond thermometer 0.1 μm in diameter has an accuracy of about 50 mK.[15] Ratiometric fluorescent thermometers of the same size have an accuracy that is about an order of magnitude lower, though the method has many practical advantages already exploited to explore, for example, the origin of thermogenesis in cells.[8] Since conclusions concerning local temperature in the cell are limited by fluctuations in temperature inherent to a small thermometer, it is worthwhile examining the properties that control its accuracy. In this article, we address the accuracy of two classes of thermometers: (1) fluorescent dyes, of the kind used in polymer dye thermometers,[5] fluorescent proteins,[7] and ratiometric studies,[8] in which the fluorescence of at least one dye inside the thermometer depends on temperature; (2) solid state thermometers, such as nanodiamonds,[15] in which the energy splitting of spin states depends on temperature.

To examine the system-specific properties that influence fluctuation in temperature measured by these two classes of nanoscale thermometers we adopt the spin-boson model, which describes the interaction between the states of the thermometer, taken for simplicity as a two-level system, and its local dissipative environment. The spin-boson model,[16,17] widely used to describe, for example, electron transfer in the condensed phase,[18,19] electronic conduction in molecules,[20] and thermal transport,[21] provides a convenient starting point to examine the origin of temperature fluctuations inherent to nanoscale thermometers and the extent to which they might be reduced. We shall see that even this simple model predicts very well the temperature fluctuations of a number of small thermometers observed in recent experiments. All parameters required to estimate the accuracy can be calculated for the specific systems of interest, as we illustrate in the examples below.

In the following section we describe the theoretical model for calculating the accuracy of fluorescent polymers and proteins and for solid-state nanothermometers. In section 3 we present the results of calculations using the model for both classes of thermometers, and discuss the size-dependence and other system properties that influence the temperature fluctuations. We conclude in section 4.

2. THEORETICAL MODELS

2.A. Fluorescent Polymers and Proteins. We consider a two-level system (TLS) split by energy, ε, coupled linearly to a bath of N oscillators, which we refer to as the local bath (LB). The TLS represents two conformational states of the fluorescent thermometer, the LB corresponds to the modes of the dyes and polymeric material that encapsulates the dye. The oscillators are also coupled to each other and to the cellular environment. For the TLS coupled to the LB we have

Special Issue: Branka M. Ladanyi Festschrift

Received: August 8, 2014
Revised: September 23, 2014
Published: September 26, 2014

   dx.doi.org/10.1021/jp508047q | J. Phys. Chem. B 2015, 119, 9000−9005

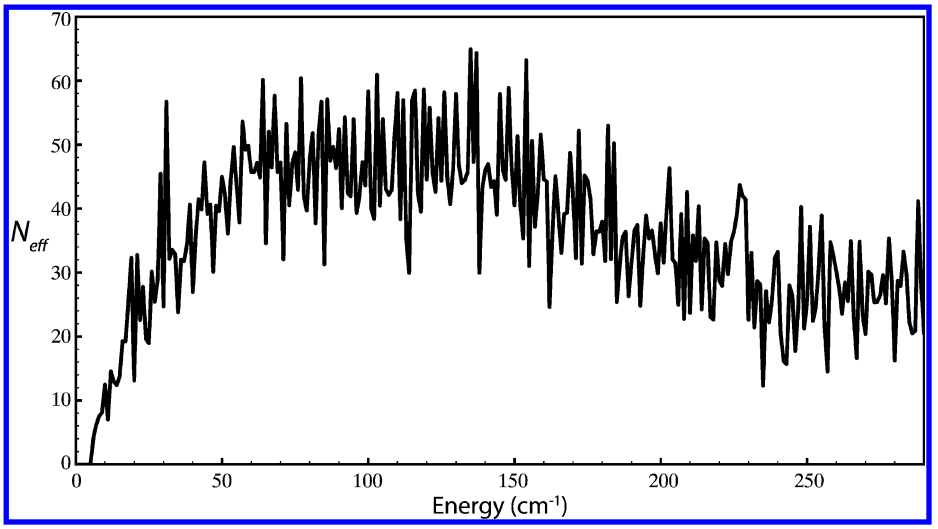

Figure 1. N_{eff} calculated for GFP.

$$H = \frac{\varepsilon}{2}\sigma_z + \sum_{k=1}^{N} \varepsilon_k a_k^{\dagger} a_k + \sigma_x X \tag{1a}$$

$$X = \sum_{k=1}^{N} f_k (a_k + a_k^{\dagger}) \tag{1b}$$

We assume that the initial state of the total system is a product of an arbitrary state of the TLS and the equilibrium state of the LB. Under the weak TLS-LB coupling assumption the TLS is driven to equilibrium, diagonal in the σ_z basis, via coupling to N_{eff} oscillators of the LB. We shall be more specific about the effective number of oscillators, N_{eff}, below, and provide a more detailed justification in the appendix. The picture is that the N_{eff} oscillators resonantly couple to the two levels split by ε, which correspond to those states, k, with energy, $\varepsilon_k \approx \varepsilon$, within a characteristic line width, γ_k; we denote $\gamma_k = \gamma$ for simplicity. The line width is the result of nonlinear coupling of the oscillators of the LB to each other via anharmonic interactions that do not explicitly appear in eq 1, such as those that give rise to intramolecular vibrational redistribution,[22−24] and coupling to its environment, for example, the cell.

For the thermometer to be sensitive to changes in the population of the TLS with changes in temperature we assume $\varepsilon < k_B T$, where k_B is Boltzmann's constant. Let $\langle n \rangle$ be the average number of vibrational quanta in the oscillators of the LB with energy near ε, which at temperature, T, we take to be given by the Planck distribution, $\langle n \rangle = (e^{\varepsilon/k_B T} - 1)^{-1}$. We calculate the variance in temperature, $(\delta T)^2$, as

$$(\delta T)^2 = \left(\frac{\varepsilon}{k_B}\right)^2 \left\langle \left(\frac{1}{N_{\text{eff}}} \sum_{k \in I} (n_k - \langle n \rangle) \right)^2 \right\rangle \tag{2}$$

where I is the set of all levels, k, that fall within the line width, γ, for $\varepsilon_k \approx \varepsilon$. Since the occupation numbers of each oscillator are not correlated,

$$(\delta T)^2 = \left(\frac{\varepsilon}{k_B}\right)^2 \frac{1}{N_{\text{eff}}} (\langle n^2 \rangle - \langle n \rangle^2) \tag{3}$$

Because $\varepsilon < k_B T$, we have

$$\langle n^2 \rangle - \langle n \rangle^2 = \langle n \rangle (1 + \langle n \rangle) \approx \langle n \rangle^2 \approx \left(\frac{k_B T}{\varepsilon}\right)^2 \tag{4}$$

so that

$$\frac{\delta T}{T} \approx \frac{1}{N_{\text{eff}}^{1/2}} \tag{5}$$

as we would expect from the central limit theorem.

The accuracy is thereby determined by the number of effective oscillators, N_{eff}, within γ of ε. In practice we take

$$N_{\text{eff}} \approx \gamma \rho(\varepsilon) \tag{6}$$

where $\rho(\varepsilon)$ is the number of vibrational modes per unit energy of the thermometer. A typical line width corresponds to a vibrational lifetime of order 1 ps, so is of order 1 cm^{-1}. We shall use for a specific example the lifetimes of the vibrational modes of green fluorescent protein (GFP), which we present below. At low energy, corresponding to $\varepsilon < k_B T$, the vibrational density of states of GFP is 1−10/cm^{-1}.[25] The number of modes per unit frequency also depends on the dye, fluorescent polymer or fluorescent protein that is used. Again, we use the vibrational density of states of GFP as a specific example and scale the size of the system based on the protein density, which is about 1.3 g cm^{-3}, comparable to the density, 1.2 g cm^{-3}, of the PMMA embedding the fluorescent dyes of the ratiometric thermometer.[8] Since the radius of gyration of GFP is 2.0 nm,[26] we estimate N_{eff} for a thermometer of radius, r (nm), by rescaling the GFP value as

$$N_{\text{eff}} = \gamma \rho_{\text{GFP}}(\varepsilon) \left(\frac{r}{2.0}\right)^3 \tag{7}$$

2.B. Solid State Nanoscale Thermometers. We consider a two-level system (TLS) model that captures the mechanism of a nanoscale diamond thermometer. The excited spin states based on nitrogen vacancy are in fact doubly degenerate[15] and the model we present here captures the effect of temperature on the splitting of the ground and (degenerate) excited spin states. The energy splitting, ε, is tuned by the elastic properties of the material, which in turn depends on temperature, that is, the changes in the splitting, $\Delta\varepsilon$, are temperature-dependent. For a solid state LB, a distortion localized in space leads to a uniform contribution from all delocalized phonon modes, that

dx.doi.org/10.1021/jp508047q | J. Phys. Chem. B 2015, 119, 9000−9005

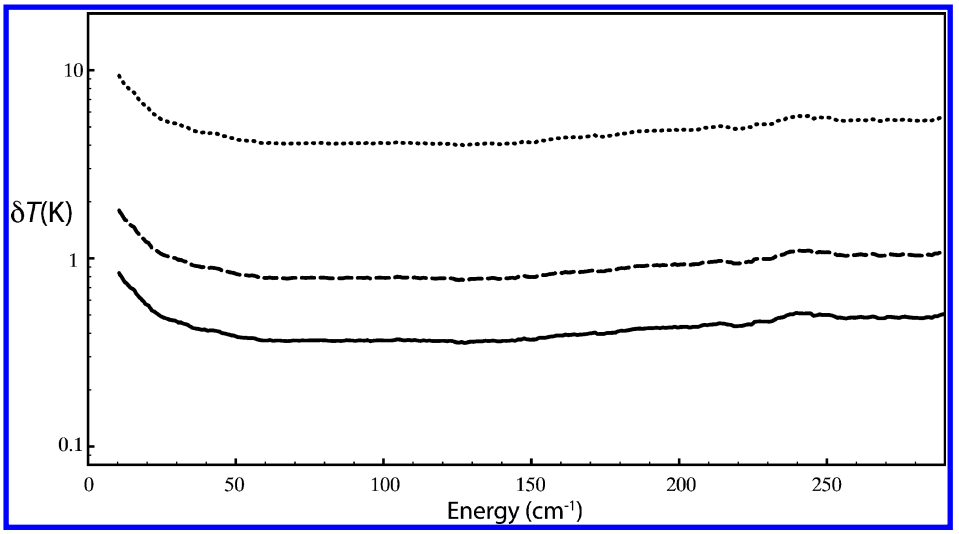

Figure 2. Accuracy, δT, at 310 K as a function of ε for a fluorescent organic thermometer of radius 10 (dots), 30 (dashes), and 50 nm (solid).

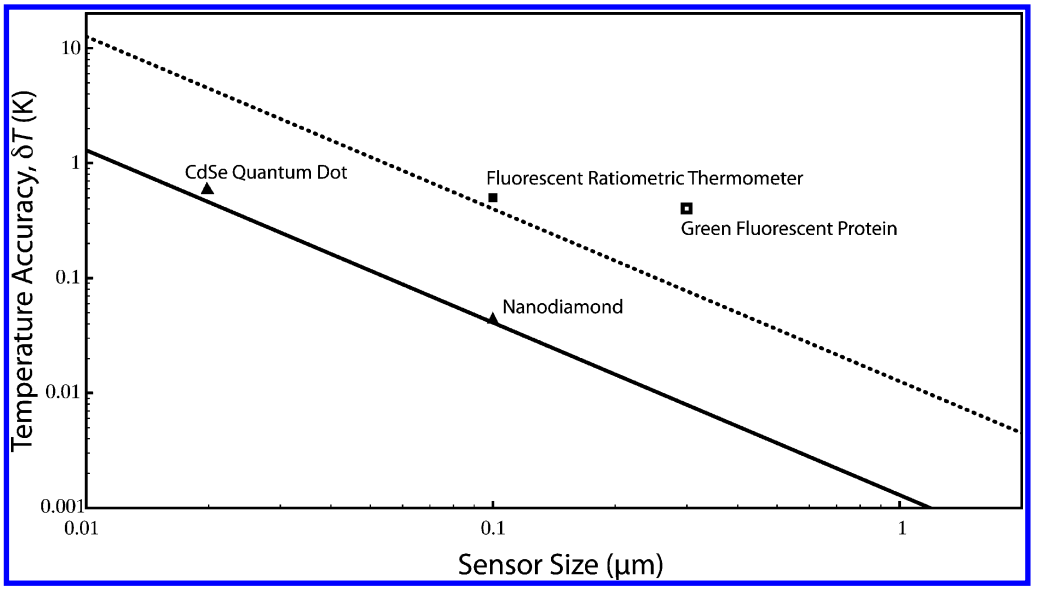

Figure 3. Accuracy, δT, at 310 K as a function of thermometer size (diameter) for the fluorescent organic thermometers (dashed line) and solid-state thermometers (solid line) predicted with eqs 7 and 12, respectively. Experimental results for solid state (diamonds) and organic (squares) thermometers were obtained from ref 15 (diamonds), ref 12 (quantum dots), ref 8 (ratiometric fluorescent thermometer), and ref 7 (GFP). The latter, indicated with an open symbol, represents the diffraction limited spatial resolution reported,[7] not the actual size of the thermometer (see text).

is, f_k in eq 1b is $|f_k| = (3N_A)^{-1/2}$, where N_A is the number of atoms in the sample. Since the energy shift, $\Delta\varepsilon$, varies for small distortion, x, as $\Delta\varepsilon = Bx^2$, where B is a constant, the energy shift is

$$\Delta\varepsilon = B\left\langle \frac{1}{3N_A}\sum_{k=1}^{3N_A} a_k^{\dagger}a_k \right\rangle \tag{8}$$

For a solid state thermometer (like the N−V center in diamond) most of the modes possess frequencies close to the Debye frequency, $\omega_D = k_B T_D/\hbar$. The average mode energy, using the Debye relation for the mode density, is $\varepsilon_k \approx 3k_B T_D/4$. Then if the Debye temperature is much larger than 300 K (for diamond it is 1860 K), we have $\langle n_k\rangle = \langle a_k^{\dagger}a_k\rangle \approx e^{-3T_D/4T}$, so that

$$\Delta\varepsilon \approx Be^{-3T_D/4T} \tag{9}$$

When $T < T_D$, we can approximate the variance in the number of phonons as

$$\langle n_k^2\rangle - \langle n_k\rangle^2 = \langle n_k\rangle(1 + \langle n_k\rangle) \approx \langle n_k\rangle \approx e^{-3T_D/4T} \tag{10}$$

Then

$$\frac{\delta(\Delta\varepsilon)}{\varepsilon} = \frac{1}{\sqrt{3N_A}}\frac{B\sqrt{\langle n_k^2\rangle - \langle n_k\rangle^2}}{B\langle n_k\rangle} = \frac{e^{3T_D/8T}}{\sqrt{3N_A}} \tag{11}$$

One can now compute relative fluctuations of temperature using the identity $d(\Delta\varepsilon) = \Delta\varepsilon(3T_D/4T^2)dT$. Therefore

$$\frac{\delta T}{T} = \left(\frac{4T}{3\sqrt{3}\,T_D}e^{3T_D/8T}\right)\frac{1}{\sqrt{N_A}} \tag{12}$$

The term in parentheses is in practice close to 1 when $T \approx 300$ K. For diamond, with a high Debye temperature of 1860 K, the term in parentheses is 1.27. (For a solid with a low Debye temperature of, say 100 K, the term in parentheses is 0.87.) Therefore, near 300 K, the accuracy is close to $T/(N_A)^{1/2}$.

dx.doi.org/10.1021/jp508047q | J. Phys. Chem. B 2015, 119, 9000−9005

3. RESULTS AND DISCUSSION

3.A. Fluorescent Polymers and Proteins. In Figure 1 we plot N_{eff} for GFP (r = 2 nm) as a function of frequency of the LB calculated with eq 7 to ≈300 cm^{-1}, that is, to ≈450 K. This range includes all temperatures that the thermometers, designed to probe local temperature of the cell, would be typically applied. For N_{eff} of GFP, we use the vibrational density of states of GFP presented previously,[25] which is similar to the vibrational density of states of many proteins.[27,28] The line width, γ, is given by $\gamma = \hbar/2\tau$, where τ^{-1} is the mode damping rate, which was calculated quantum mechanically for all modes of GFP by including third order anharmonic interactions using first order time-dependent perturbation theory.[25,29] Similar mode frequency-dependent decay rates have been calculated for other proteins.[30−32] The computed results compare well with experimental measurements where comparisons can be made,[33−36] and they are comparable to lifetimes of other peptides and large organic molecules that have been computed and measured.[37−40] We observe that N_{eff} rises at low energy to about 50 near $\varepsilon \approx 50$ cm^{-1}, beyond which it does not vary much. Since the accuracy of a thermometer varies as $N_{eff}{}^{-1/2}$ we do not expect much ε-dependence except perhaps at very small ε.

In Figure 2 we present results calculated with eqs 5 and 7 for the accuracy of a nanothermometer of radius 10, 30, and 50 nm at T = 310 K. The r = 50 nm thermometer corresponds to the average radius of the ratiometric thermometers presented in ref 8. We see that for that size the accuracy is ≈0.4−1.0 K, depending on the energy splitting, ε. Therefore, this splitting has, in practice, only a small effect on the thermometer's accuracy. The accuracy that we obtain with the model, parametrized by calculations of the vibrational density of states and line widths of GFP, is consistent with experimental measurement using ratiometric fluorescent thermometers of radius around 50 nm, where an accuracy of about 0.5 °C was reported.[8]

3.B. Nanoscale Diamonds. For a diamond (density ≈3.5 g cm^{-3}) thermometer of radius 50 nm, $N_A \approx 9.2 \times 10^7$ so that at 310 K we estimate with eq 12 the accuracy to be 41 mK, in excellent agreement with the reported value of 44 mK.[15] The nanoscale diamond and organic thermometers discussed in the previous section are the same size but their accuracy differs by an order of magnitude.

We generalize our results for thermometer accuracy in Figure 3, where we plot the size-dependence of the accuracy at 310 K for the solid-state thermometer using eq 12 and the fluorescent organic thermometer using eq 7. We compare with experimental results for the nanoscale diamond,[15] the ratiometric fluorescent thermometer,[8] and the quantum dot thermometer.[12] For the latter we plot the intrinsic temperature accuracy of the quantum dot, ≈ 0.6 K, not the overall accuracy of the quantum dot in the cell, which was determined to be ≈2 K, a greater uncertainty due to movement of the quantum dot in the cell.[12] The predictions of our model fit the data for both the solid state and the fluorescent organic thermometers well.

For the quantum dot, nanodiamond, and ratiometric fluorescent thermometer the size indicated corresponds to the diameter of the thermometer. For the ratiometric fluorescent thermometer, for example, the polymer casing that encloses the dyes, which together correspond to ≈100 nm in diameter,[8] provides a clear boundary for the thermometer. We have added a second organic thermometer in Figure 3 where the boundary is less clear. The temperature accuracy of the GFP thermometer is reported for a diffraction-limited region of about 300 nm.[7] The "size" reported is thus different than for the other thermometers, which we indicate with an open symbol in Figure 3, as opposed to filled for the others. The reported accuracy of 0.4 K can thus only be indirectly and loosely compared with the present theory. To obtain the calibration curves in ref 7 a 3×10^{-5} M GFP solution was used, which corresponds to about 255 GFP molecules in the diffraction limited region. If we scale the accuracy by $N^{-1/2}$, where N is the number of GFP molecules in the region, we expect an accuracy of 6−7 K, which corresponds to a thermometer of diameter ≈15 nm, much greater than the ≈4 nm diameter of GFP. Allowing for a larger effective diameter, due to dynamic coupling to the hydration layer around the protein,[41−44] it could be argued that a single GFP thermometer extends to ≈6 nm. In that case, for the concentrations used in the calibration study in ref 7, an accuracy of $\delta T \approx 1.7$ K would be expected, larger than the 0.4 K reported.

The discussion above has focused on the role of size in the accuracy of two classes of thermometers. There are of course likely to be other sources of error that reduce the accuracy, such as background signal from the environment. In this respect the size-dependence provides a lower bound on δT. Signal to noise improves with longer observation time, so that accuracy also depends on measurement time, which was taken to be instantaneous in the above estimates. While some effects of observation time depend on the environment of the thermometer that is probed, others depend on the thermometer itself. For measurement times, t_M, much longer than thermal relaxation times of the thermometer, t_F, the accuaracy becomes $\delta T/T = (1/N_{eff}^{1/2})(t_F/t_M)^{1/2}$. The thermal relaxation time, t_F, depends on the thermal diffusivity, D_T, of the thermometer and the thermal boundary conductance, h, between the thermometer and its environment.[45] For example, for proteins D_T is of order 0.1 nm^2 ps^{-1}. Neglecting boundary conductance for simplicity (though its effect on thermal transport may be comparable to thermal diffusion in the thermometer, as is the case for proteins[46]), t_F is of order r^2/D_T, so for $r \approx 50$ nm the measurement time, t_M, needs to be at least 0.1 μs to significantly improve accuracy.

4. CONCLUDING REMARKS

A variety of nanoscale thermometers recently developed and applied to measure local temperature within a living cell include fluorescent polymers[5,6] and proteins,[7] ratiometric fluorescent thermometers,[8] polymer dots,[9] fluorescent nanoparticles,[10,11] quantum dots,[12−14] and nanoscale diamonds.[15] Their utility depends on how easily they can be introduced into the cell as well as their resolution. We have calculated the accuracy of fluorescent polymer, protein and solid-state nanothermometers adopting the spin-boson model.

The accuracy varies as $N_{eff}{}^{-1/2}$ for each class of thermometer. For organic thermometers N_{eff} corresponds to the product of the vibrational density of states and the line-width of oscillators of the local bath to which the thermometer is coupled. As we observe from our calculation for green fluorescent protein, this product does not vary much with the energy splitting between different conformational states of the thermometer. In practice, the accuracy is controlled by the size, for instance, the radius, r, of the thermometer, and varies as $r^{-3/2}$. For many solid-state thermometers $N_{eff} \approx N_A$, where N_A is the number of atoms in the thermometer. As with organic thermometers the accuracy

dx.doi.org/10.1021/jp508047q | J. Phys. Chem. B 2015, 119, 9000−9005

varies as $r^{-3/2}$, but is typically better by about an order of magnitude.

Both quantum dot[12] and ratiometric fluorescent[8] nanoscale thermometers developed to measure local temperature in the cell indicate heterogeneous heat production during thermogenesis resulting from ionomycin-induced Ca^{2+} bursts. Those measurements reveal an average increase of roughly 2 °C, which both kinds of thermometers can resolve, though much of the variation in temperature around the average observed for individual measurements may be inherent to the finite-size of the thermometers.

The possibility of subcellular temperature gradients for signaling and regulation in cells has been raised,[12] which can be further explored as more accurate measurements of local temperature inside the cell become possible. Models assuming homogeneous thermal flow inside the cell have been shown to be inconsistent with the sizable increase in temperature observed with ionomycin-induced Ca^{2+} bursts.[8] To model signaling as the result of any local temperature gradient information would be needed about thermal transport within the cell. At a local level this information could include, for example, thermal transport in proteins,[30,47,48] recently measured,[49] and thermal conductance between proteins and water.[46,50−52] Signaling pathways resulting from any subcellular thermal gradients may eventually be probed on even smaller length and shorter time scales with molecular thermometers based on ultrafast vibrational spectroscopy.[53−57]

APPENDIX

Our estimate for the effective number of oscillators, $N_{\text{eff}} = \gamma\rho(\varepsilon)$, used in eq 6 can be derived more explicitly than presented in section 2.A. For the TLS-LB system defined by eq 1 the ratio of the population of the excited to the ground state is given by[58,59]

$$\frac{p_e}{p_g} = \frac{R(-\varepsilon)}{R(\varepsilon)} = e^{-\varepsilon/k_B T} \tag{A1}$$

Here $R(\varepsilon)$ is the Fourier transform of the autocorrelation function

$$R(\varepsilon) = \int_{-\infty}^{\infty} e^{i\varepsilon t/\hbar}\langle X(t)X\rangle \mathrm{d}t \tag{A2}$$

To compute the spectral density $R(\varepsilon)$ we use the following phenomenological expression for the correlation functions, which takes into account damping of the LB modes,

$$\langle a_k^{\dagger} a_l\rangle = \delta_{kl} e^{i\varepsilon_k t/\hbar} e^{-\gamma_k t/\hbar}\langle n_k\rangle \tag{A3}$$

Then $(\varepsilon \geq 0)$

$$R(\varepsilon) = \sum_{k=1}^{N} |f_k|^2 \frac{\gamma_k}{(\varepsilon - \varepsilon_k)^2 + \gamma_k^2}(\langle n_k\rangle + 1) \tag{A4}$$

$$R(-\varepsilon) = \sum_{k=1}^{N} |f_k|^2 \frac{\gamma_k}{(\varepsilon - \varepsilon_k)^2 + \gamma_k^2}\langle n_k\rangle \tag{A5}$$

We assume that the coupling constants $|f_k|$ are almost uniform within γ of ε_k.

AUTHOR INFORMATION

Corresponding Authors

*E-mail: fizra@univ.gda.pl.

*E-mail: dml@unr.edu.

Notes

The authors declare no competing financial interest.

ACKNOWLEDGMENTS

This work was carried out while the authors were Senior Fellows at the Freiburg Institute for Advanced Studies (FRIAS). The authors thank Hermann Grabert, Florian Mintert, and Gerhard Stock for their hospitality and numerous stimulating discussions. Support from the National Science Foundation (NSF CHE-1361776) to D.M.L. is gratefully acknowledged.

REFERENCES

(1) Lee, J.; Kotov, N. A. Thermometer Design at the Nanoscale. *Nano Today* **2007**, *2*, 48−51.

(2) Yue, Y.; Wang, X. Nanoscale Thermal Probing. *Nano. Rev.* **2012**, *3*, 11586.

(3) Brites, C. D.; Lima, P. P.; Silva, N. J.; Millan, A.; Palacio, V. S.; Carlos, L. D. Thermometry at the Nanoscale. *Nanoscale* **2012**, *4*, 4799−4829.

(4) Ozawa, T.; Yoshimura, H.; Kim, S. B. Advances in Fluorescence and Bioluminescence Imaging. *Anal. Chem.* **2013**, *85*, 590−609.

(5) Okabe, K.; Inada, N.; Gota, C.; Harada, Y.; Funatsu, T.; Uchiyama, S. Intracellular Temperature Mapping with a Fluorescent Polymeric Thermometer and Fluorescence Lifetime Imaging Microscopy. *Nat. Commun.* **2012**, *3*, 705.

(6) Tsuji, T.; Yoshida, S.; Yoshida, A.; Uchiyama, S. Cationic Fluorescent Polymeric Thermometers with the Ability to Enter Yeast and Mammalian Cells for Practical Intracellular Temperature Measurements. *Anal. Chem.* **2013**, *85*, 9815−9823.

(7) Donner, J. S.; Thompson, S. A.; Kreuzer, M. P.; Baffou, G.; Quidant, R. Mapping Intracellular Temperature Using Green Fluorescent Protein. *Nano Lett.* **2012**, *12*, 2107−2111.

(8) Takai, Y.; Arai, S.; Murata, A.; Takabayashi, M.; Oyama, K.; Ishiwata, S.; Takeoka, S.; Suzuki, M. A Nanoparticle-Based Ratiometric and Self-Calibrated Fluorescent Thermometer for Single Living Cells. *ACS Nano* **2014**, *8*, 198−206.

(9) Ye, F.; Wu, C.; Jin, Y.; Chan, Y. H.; Zhang, X.; Chiu, D. T. Ratiometric Temperature Sensing with Semiconducting Polymer Dots. *J. Am. Chem. Soc.* **2011**, *133*, 8146−8149.

(10) Vetrone, F.; Naccache, R.; Zamarron, A.; Fuente, A. J. d. l.; Sanz-Rodriguez, F.; Maestro, L. M.; Rodriguez, E. M.; Jaque, D.; Sole, J. G.; Capobianco, J. A. Temperature Sensing Using Fluorescent Nanothermometers. *ACS Nano* **2010**, *4*, 3254−3258.

(11) Fischer, L. H.; Harms, G. S.; Wolfbeis, O. S. Upconverting Nanoparticles for Nanoscale Thermometry. *Angew. Chem., Int. Ed.* **2011**, *50*, 4546−4551.

(12) Yang, J.; Yang, H.; Lin, L. Quantum Dot Nano Thermometers Reveal Heterogeneous Local Thermogenesis in Living Cells. *ACS Nano* **2011**, *5*, 5067−5071.

(13) Albers, A. E.; Chan, E. M.; McBride, P. M.; Ajo-Franklin, C. M.; Cohen, B. E.; Helms, B. A. Dual-Emitting Quantum Dot/Quantum Rod-Based Nanothermometers with Enhanced Response and Sensitivity in Live Cells. *J. Am. Chem. Soc.* **2012**, *134*, 9565−9568.

(14) Hsia, C. H.; Wuttig, A.; Yang, H. An Accessible Approach to Preparing Water-Soluble Mn^{2+}-Doped (Cdsse)Zns (Core)-Shell Nanocrystals for Ratiometric Temperature Sensing. *ACS Nano* **2011**, *5*, 9511−9522.

(15) Kucsko, G.; Maurer, P. C.; Yao, N. Y.; Kubo, M.; Noh, H. J.; Lo, P. K.; Park, H.; Lukin, M. D. Nanometre-Scale Thermometry in a Living Cell. *Nature* **2013**, *500*, 54−58.

(16) Leggett, A. J.; Chakravarty, S.; Dorsey, A. T.; Fisher, M. P. A.; Garg, A.; Zwerger, W. Dynamics of the Dissipative Two-State System. *Rev. Mod. Phys.* **1987**, *59*, 1−85.

(17) Stock, G. A Semiclassical Self-Consistent-Field Approach to Dissipative Dynamics: The Spin-Boson Problem. *J. Chem. Phys.* **1995**, *103*, 1561−1573.

(18) Matyushov, D. V.; Ladanyi, B. M. Dispersion Solute-Solvent Coupling in Electron Transfer Reactions. I. Effective Potential. *J. Chem. Phys.* **1998**, *108*, 6362−6377.
(19) Weiss, U. *Quantum Dissipative Systems*; World Scientific: Singapore, 1999.
(20) Nitzan, A. *Chemical Dynamics in Condensed Phases*; Oxford University Press: Oxford, 2006.
(21) Segal, D. Heat Transfer in the Spin-Boson Model: A Comparative Study in the Incoherent Tunneling Regime. *Phys. Rev. E* **2014**, *90*, art. no. 012148.
(22) Stuchebrukhov, A. A.; Kuzmin, M. V.; Bagratashvili, V. N.; Letokhov, V. S. Threshold Energy Dependence of Intramolecular Vibrational Relaxation in Polyatomic Molecules. *Chem. Phys.* **1986**, *107*, 429−443.
(23) Stuchebrukhov, A. A.; Marcus, R. A. Theoretical Study of Intramolecular Vibrational Relaxation of Acetylenic CH Vibration for V = 1 and 2 in Large Polyatomic Molecules (CX3)3YCCH, Where X = H or D and Y = C or Si. *J. Chem. Phys.* **1993**, *98*, 6044−6061.
(24) Leitner, D. M.; Wolynes, P. G. Statistical Properties of Localized Vibrational Eigenstates. *Chem. Phys. Lett.* **1996**, *258*, 18−24.
(25) Leitner, D. M. Energy Flow in Proteins. *Annu. Rev. Phys. Chem.* **2008**, *59*, 233−259.
(26) Reddy, G.; Liu, Z.; Thirumalai, D. Denaturant-Dependent Folding of Gfp. *Proc. Natl. Acad. Sci. U.S.A.* **2012**, *109*, 17832−17838.
(27) Moritsugu, K.; Miyashita, O.; Kidera, A. Vibrational Energy Transfer in a Protein Molecule. *Phys. Rev. Lett.* **2000**, *85*, 3970−3973.
(28) Nishikawa, T.; Go, N. Normal Modes of Vibration in Bovine Pancreatic Trypsin Inhibitor and Its Mechanical Property. *Proteins: Struct., Funct. Genetics* **1987**, *2*, 308−329.
(29) Leitner, D. M. Mode Damping Rates in a Protein Chromophore. *Chem. Phys. Lett.* **2012**, *530*, 102−106.
(30) Yu, X.; Leitner, D. M. Vibrational Energy Transfer and Heat Conduction in a Protein. *J. Phys. Chem. B* **2003**, *107*, 1698−1707.
(31) Leitner, D. M.; Straub, J. E. *Proteins: Energy, Heat and Signal Flow*; CRC Press: Boca Raton, FL, 2009.
(32) Fujisaki, H.; Zhang, Y.; Straub, J. E. Non-Markovian Theory of Vibrational Energy Relaxation and Its Applications to Biomolecular Systems. *Adv. Chem. Phys.* **2011**, *145*, 1−34.
(33) Hamm, P.; Lim, M.; Hochstrasser, R. M. Structure of the Amide I Band of Peptides Measured by Fs Nonlinear-Infrared Spectroscopy. *J. Phys. Chem. B* **1998**, *102*, 6123−6138.
(34) Xie, A.; Meer, L. v. d.; Hoff, W.; Austin, R. H. Long-Lived Amide I Vibrational Modes in Myoglobin. *Phys. Rev. Lett.* **2000**, *84*, 5435−5438.
(35) Peterson, K. A.; Rella, C. W.; Engholm, J. R.; Schwettman, H. A. Ultrafast Vibrational Dynamics of the Myoglobin Amide I Band. *J. Phys. Chem. B* **1999**, *103*, 557−561.
(36) Cremeens, M. E.; Fujisaki, H.; Zhang, Y.; Zimmermann, J.; Sagle, L. B.; Matsuda, S.; Dawson, P. E.; Straub, J. E.; Romesberg, F. E. Efforts toward Developing Direct Probes of Protein Dynamics. *J. Am. Chem. Soc.* **2006**, *128*, 6028−6029.
(37) Nguyen, P. H.; Hamm, P.; Stock, G. Nonequilibrium Molecular Dynamics Simulation of Photoinduced Energy Flow in Peptides: Theory Meets Experiment. In *Proteins: Energy, Heat and Signal Flow*; Leitner, D. M., Straub, J. E., Eds.; CRC Press, Taylor & Francis Group: Boca Raton, FL, 2009; pp 149−168.
(38) Backus, E. H. G.; Nguyen, P. H.; Botan, V.; Pfister, R.; Moretto, A.; Crisma, M.; Toniolo, C.; Stock, G.; Hamm, P. Energy Transport in Peptide Helices: A Comparison between High- and Low-Energy Excitations. *J. Phys. Chem. B* **2008**, *112*, 9091−9099.
(39) Lin, Z.; Lawrence, C. M.; Xiao, D.; Skourtis, S. S.; Sessler, J. L.; Beratan, D. N.; Rubtsov, I. V. Modulating Unimolecular Charge Transfer by Exciting Bridge Vibrations. *J. Am. Chem. Soc.* **2009**, *131*, 18060−18062.
(40) Kayanenko, V. M.; Tesar, S. L.; Rubtsov, G. I.; Burin, A. L.; Rubtsov, I. V. Structure Dependent Energy Transport: Relaxation-Assisted 2dir Measurements and Theoretical Studies. *J. Phys. Chem. B* **2011**, *115*, 11063−11073.
(41) LeBard, D. N.; Matyushov, D. V. Ferroelectric Hydration Shells around Proteins: Electrostatics of the Protein−Water Interface. *J. Phys. Chem. B* **2010**, *114*, 9246−9258.
(42) Yu, X.; Park, J.; Leitner, D. M. Thermodynamics of Protein Hydration Computed by Molecular Dynamics and Normal Modes. *J. Phys. Chem. B* **2003**, *107*, 12820−12829.
(43) Heyden, M.; Tobias, D. J. Spatial Dependence of Protein−Water Collective Hydrogen Bond Dynamics. *Phys. Rev. Lett.* **2013**, *111*, 218101.
(44) Meister, K.; Ebbinghaus, S.; Xu, Y.; Duman, J. G.; DeVries, A.; Gruebele, M.; Leitner, D. M.; Havenith, M. Long-Range Protein−Water Dynamics in Hyperactive Insect Antifreeze Proteins. *Proc. Natl. Acad. Sci. U.S.A.* **2013**, *110*, 1617−1622.
(45) Li, P.; Champion, P. M. Investigations of the Thermal Response of Laser-Excited Biomolecules. *Biophys. J.* **1994**, *66*, 430−436.
(46) Lervik, A.; Bresme, F.; Kjelstrup, S.; Bedeaux, D.; Rubi, J. M. Heat Transfer in Protein−Water Interfaces. *Phys. Chem. Chem. Phys.* **2010**, *12*, 1610−1617.
(47) Leitner, D. M. Heat Transport in Molecules and Reaction Kinetics: The Role of Quantum Energy Flow and Localization. *Adv. Chem. Phys.* **2005**, *130*, 205−256.
(48) Yu, X.; Leitner, D. M. Heat Flow in Proteins: Computation of Thermal Transport Coefficients. *J. Chem. Phys.* **2005**, *122*, 054901−054911.
(49) Foley, B. M.; Gorham, C. S.; Duda, J. C.; Cheaito, R.; Szwejkowski, C. J.; Constantin, C.; Kaehr, B.; Hopkins, P. E. Protein Thermal Conductivity Measured in the Solid State Reveals Anharmonic Interactions of Vibrations in a Fractal Structure. *J. Phys. Chem. Lett.* **2014**, *5*, 1077−1082.
(50) Leitner, D. M. Thermal Boundary Conductance and Rectification in Molecules. *J. Phys. Chem. B* **2013**, *117*, 12820−12828.
(51) Xu, Y.; Leitner, D. M. Vibrational Energy Flow through the Green Fluorescent Proteinwater Interface: Communication Maps and Thermal Boundary Conductance. *J. Phys. Chem. B* **2014**, *118*, 7818−7826.
(52) Agbo, J. K.; Xu, Y.; Zhang, P.; Straub, J. E.; Leitner, D. M. Vibrational Energy Flow across Heme-Cytochrome C and Cytochrome C-Water Interfaces. *Theor. Chem. Acc.* **2014**, *133*, 1504.
(53) Backus, E. H. G.; Nguyen, P. H.; Botan, V.; Moretto, A.; Crisma, M.; Toniolo, C.; Zerbe, O.; Stock, G.; Hamm, P. Structural Flexibility of a Helical Peptide Regulates Vibrational Energy Transport Properties. *J. Phys. Chem. B* **2008**, *112*, 15487−15492.
(54) Müller-Werkmeister, H. M.; Bredenbeck, J. A Donor-Acceptor Pair for the Real Time Study of Vibrational Energy Transfer in Proteins. *Phys. Chem. Chem. Phys.* **2014**, *16*, 3261−3266.
(55) Lin, Z.; Rubtsov, I. V. Constant-Speed Vibrational Signaling Along Polyethyleneglycol Chain up to 60 Å Distance. *Proc. Natl. Acad. Sci. U.S.A.* **2012**, *109*, 1414−1418.
(56) Botan, V.; Backus, E. H. G.; Pfister, R.; Moretto, A.; Crisma, M.; Toniolo, C.; Nguyen, P. H.; Stock, G.; Hamm, P. Energy Transport in Peptide Helices. *Proc. Natl. Acad. Sci. U.S.A.* **2007**, *104*, 12749−12754.
(57) Helbing, J.; Devereux, M.; Nienhaus, K.; Nienhaus, G. U.; Hamm, P.; Meuwly, M. Temperature Dependence of the Heat Diffusivity of Proteins. *J. Phys. Chem. A* **2012**, *116*, 2620−2628.
(58) May, V.; Kühn, O. *Charge and Energy Transfer Dynamics*, 3rd ed.; Wiley-VCH: Weinheim, 2011.
(59) Breuer, H.-P.; Petruccione, F. *The Theory of Open Quantum Systems*; Oxford University Press: Oxford, U.K., 2002.